Oscillatory Marangon Flow in Half-Zone Liquid Bridge of Molten Tin

By

N. Imaishi[1], K. Li[1], S. Yasuhiro[1], S. Yoda[2]

Abstract: To evaluate the experimental observations at JAXA, a long-run numerical simulation was conducted on a realistic model of a half-zone liquid bridge of molten tin, which is identical to the apparatus of the JAXA's experiment. Using time dependent temperature difference imposed on both ends of the supporting rods, which is calculated based on the experimental temperature recordings measured through two thermocouples, the numerical results reproduce the experimentally observed oscillations of melt free surface temperature with different frequencies and explain the experimental results. The present study also indicates that very sensitive temperature measuring system must be developed to experimentally determine the critical conditions of Marangoni flow transitions through the melt free surface temperature measurements.

1. Introduction

Studies on stability of Marangoni flow in half-zone liquid bridges of low-Pr fluid are stimulated by the experimental fact that Marangoni flow instability in floating zones may cause striations in crystals grown in space [1]. It is well known that in half-zone liquid bridges of low-Pr fluid, Marangoni flow is axisymmetric and steady under a small temperature difference (ΔT). At a certain threshold value of ΔT (the first critical ΔT_{c1}), a transition to a three-dimensional steady Marangoni flow occurs. At a further higher threshold value of ΔT (the second critical ΔT_{c2}), a second transition to oscillatory Marangoni flow occurs. Many experimental studies were conducted on the Marangoni flow in half-zone liquid bridges over a wide range of Pr number. However, few [2-15] have been reported on low-Pr fluids due to the difficulties in conducting well-controlled experiments induced by the opacity, high reactivity with oxygen and high melting temperatures of the low-Pr fluids (mostly liquid metals). On the other hand, theoretical studies conducted on the Marangoni flow in half-zone liquid bridges of low-Pr fluid, both linear stability analyses [16-22] and direct numerical simulations [22-30], confirmed the two-step transition. In the numerical studies, a simple liquid bridge model was adopted, i.e., the liquid bridge was supported between two differentially heated isothermal discs and the calculation domain was restricted to the melt zone.

Recently, JAXA conducted on-ground experiments [31] on incipience of the oscillatory Marangoni flow in a small size liquid bridge of molten tin supported by iron rods. The imposed temperature difference on the liquid bridge was measured through two fine thermocouples mounted in the rods ($\Delta T'$). The thermocouple junction was located on the axis of the supporting rods with a certain distance ($d = 0.5mm$) apart from the melt/rod interface. By measuring the melt free surface temperatures at two different points through radiation pyrometers, the oscillations of melt free surface temperatures were successfully detected. However, the detected temperature oscillations are low with large amplitude. The frequencies are much lower than the critical frequencies predicted

---

[1]Institute for Materials Chemistry and Engineering, Kyushu University, Fukuoka, Japan
[2]JAXA, Sengen, Tsukuba, Japan

by the numerical simulations. Moreover, the critical Marangoni numbers based on $\Delta T'$ are larger than the numerical predicted ones by a factor of 1.5 to 2.0 . It is noted that for such a low-Pr fluid liquid bridge apparatus, the thermal conductivity of the supporting iron rods (k_r) is smaller than that of the molten tin (k). The large heat flux through the rods and melt zone may cause significant temperature drops even if the thermocouples position offsets (d) are small. So $\Delta T'$ may not correctly represent the effective temperature difference which drives the Marangoni flow. On the other hand, there remains a question about the observability of the critical point, i.e., the incipience of the oscillatory disturbances. In the experiment, the imposed temperature difference was gradually increased and the oscillatory disturbances started growth process after the critical condition was satisfied. Thus, the observed critical condition may substantially larger than the theoretical one. However, the above aspects have not been studied in detail so far except in our previous study on a liquid bridge of As = 2.0 [32].

In present study, a long-run numerical simulation was conducted on a realistic model of the half-zone liquid bridge of motlen tin to precisely review the JAXA experiment on a liquid bridge of As = 1.22 [31]. The numerical results reproduce the experimentally observed supercritical melt free surface temperature oscillations of different frequencies and explain the experimental results. The present study also gives the first and second critical Marangoni numbers and indicates that very sensitive temperature measuring system is necessary to be developed to detect the temperature oscillations right after the incipience of the oscillatory Marangoni flow experimentally. The numerical results are described in the dimensional form for the convenient comparison with the experiment results.

2. Problem statement

The schematics of the half-zone liquid bridge model adopted in the present study are shown in Fig.1. The gravity level is assumed to be zero because the dynamic Bond number of the liquid bridge in the experiment is smaller than unity, so the melt free surface is assumed to be non-deformable and cylindrical. A cylindrical coordinate system (r, θ, z) is adopted here with the origin of the coordinate located at the center of the lower melt/rod interface. The radius of the liquid bridge is R. The length of the melt zone is L and the length of iron rod is L_r. The thermocouple junctions are located on the axis of the supporting rods with certain distance d apart from the melt/rod interfaces. The aspect ratios are defined as: As = L/R, $As_r = L_r/R$ and $As_d = d/R$ respectively. The fluid being considered is molten tin of Pr = 0.009. It is assumed to be an incompressible Newtonian fluid with constant properties. With the above assumptions, the fundamental equations are expressed in dimensional form as follows:

In the liquid bridge:

$$\nabla \cdot U = 0 \tag{1}$$

$$\frac{\partial U}{\partial t} + U \cdot \nabla U = -\frac{1}{\rho} \nabla p + \nu \nabla^2 U \tag{2}$$

$$\frac{\partial T}{\partial t} + U \cdot \nabla T = \alpha \nabla^2 T \tag{3}$$

In the iron rods,

$$\frac{\partial T}{\partial t} = \alpha_r \nabla^2 T \tag{4}$$

where $U = (U_r, U_\theta, U_z)$ is the velocity vector, v the kinematic viscosity, t time, ρ the density, p pressure, T temperature and α the thermal diffusivity for fluid, α_r the thermal diffusivity for rod respectively. The fluid is assumed to be motionless and isothermal before the temperature difference between the supporting iron rods is imposed.

The boundary conditions are defined as follows:
At the free surface of the liquid bridge (r = R):

$$U_r = 0, \quad \frac{\partial}{\partial r}\left(\frac{U_\theta}{r}\right) = -\frac{\sigma_T}{r^2 \rho v}\frac{\partial T}{\partial \theta}, \quad \frac{\partial U_z}{\partial r} = -\frac{\sigma_T}{\rho v}\frac{\partial T}{\partial z}, \quad \frac{\partial T}{\partial r} = 0 \tag{5}$$

At the surface of the rods (r = R):

$$\frac{\partial T}{\partial r} = 0 \tag{6}$$

At the upper and lower melt/rod interface (z = L and z = 0):

$$U_r = U_\theta = U_z = 0, \quad k\frac{\partial T}{\partial z} = k_r\frac{\partial T}{\partial z} \tag{7}$$

where k and k_r are the heat conductivity for the rod and melt respectively. A simple heat conduction dominant model [33] is employed to convert the thermocouple temperature recordings T_1 (thermocouple-1) and T_2 (thermocouple-2) to the time dependent temperatures imposed on the hot end (T_H) and cold end (T_C), i.e., the heat flux through the rods and melt zone is assumed to be one-dimensional in axial direction, steady and totally governed by heat conduction. The heat conduction dominant model gives the follows,

$$T_H = T_1 + \Delta T'\left(\frac{(L_r - d)}{\frac{k_r}{k}L + 2d}\right), \qquad T_C = T_2 - \Delta T'\left(\frac{(L_r - d)}{\frac{k_r}{k}L + 2d}\right) \tag{8}$$

where $\Delta T' = T_1 - T_2$. As mentioned above, $\Delta T'$ does not precisely represent the effective temperature difference driving the Marangoni flow, thus the effective temperature difference acting on the liquid bridge melt/solid interfaces is introduced as follows,

$$\Delta T_e = \left\{\int_0^{2p} T(R, \theta, 0)\,d\theta - \int_0^{2p} T(R, \theta, L)\,d\theta\right\}\Big/2p \tag{9}$$

The Prandtl number and the Marangoni number referred in the present study are defined as:

$$Pr = \frac{v}{\alpha}, \quad Ma = -\frac{R\sigma_T\Delta T_e}{\rho v\alpha}.$$

3. Numerical methods

The governing equations are discretized by the finite difference method with a Kawamura scheme of third order accuracy for the convective terms [34]. Non-uniform staggered grids are adopted to increase the resolution near the boundary. The radial velocities at the central axis are calculated by the method of Ozoe et al. [35]. A fully implicit code is developed based on the preconditioned Bi-CGSTAB method [36]. The details of the numerical method can be found elsewhere [27-30]. In the present study, the total grid number is 27×63×94 (N_r ×N_θ×N_z), and 40 grids are placed in the z-direction of the melt zone. The numerical simulation was carried on a vector processor of Fujitsu VPP-5000. The thermophysical properties and geometric parameters for the liquid bridge model are listed in Table 1, which are identical to the experiment conditions.

4. Results

As shown in Fig.2, the experimental temperature recordings of the thermocouples are simplified to be linear with a constant heating velocity ($d\Delta\mathrm{T}'/dt$ = 0.34 K/min, i.e., Case-1 hereafter), which is the same as the experimental averaged heating velocity. The temperatures at the hot and cold ends calculated by the heat conduction dominant model are also shown in Fig.2, and taken as the thermal boundary conditions for the simulation. To evaluate the effect of the heating velocity on the incipience of the critical conditions, the calculation with a faster heating velocity ($d\Delta\mathrm{T}'/dt$ = 2.04 K/min, i.e., Case-2 hereafter) was also conducted.

For case-1, Fig.3 shows the evolution of maximum absolute value of the radial velocity at the axis ($\left. \left| \mathrm{U}_{r(r=0,=0.5\mathrm{L})} \right| \right|_{\max}$, i.e., indicator velocity hereafter), which is the most sensitive parameter for current oscillatory transition, against the temperature difference between the hot and cold ends ($\Delta\mathrm{T} = \mathrm{T_H} - \mathrm{T_C}$). In the early stage, the temperature and flow fields are steady and axisymmetric with a small $\Delta\mathrm{T}$, and the corresponding azimuthal velocities of four monitor points at the melt free surface are zero (see Fig.4). When $\Delta\mathrm{T}$ is increased, the amplitude of the indictor velocity increases gradually. At $\Delta T = 7.89$ K ($t = 303.5$ s), the azimuthal velocities of the monitor points start increasing quickly from zero indicating the growth of three-dimensional disturbance. The flow pattern change also results in the sudden decrease of the indicator velocity. When $\Delta\mathrm{T}$ is further increased, the three-dimensional disturbance reaches the fully developed stage, and the azimuthal velocities decrease slowly. The corresponding three-dimensional temperature and flow fields are steady with the characterized azimuthal wave number $m = 2$ (see Fig.5), and maintained during the disturbance growth process. At $\Delta\mathrm{T} = 43.05$ K ($t = 1655.2$ s), the indicator velocity starts oscillation with a frequency of $f = 0.54$ Hz by FFT analysis (see Fig.6). As shown in Fig.7, its amplitude grows exponentially and its frequency increases to $f = 1.13$ Hz (It is noted that because of the absolute value function in the definition of the indicator velocity, soon after the incipience of the oscillatory transition, the frequency of the indicator velocity is two times of the corresponding frequency of the flow field oscillation). The corresponding oscillation mode is 2+1 [30], i.e., the superimposition of $m = 1$ type three-dimensional oscillatory disturbance on the three-dimensional steady flow $m = 2$. It results in an oscillatory radial velocity on the axis. Since $\Delta\mathrm{T} = 49.4$ K ($t = 1900$ s), the oscillatory flow reaches the fully developed stage. During the time period ($t = 1900 \sim 2100$ s), the amplitude of the indicator velocity is slightly increased as shown in Fig.6, and the corresponding frequency is nearly constant (see Fig.8). On the other hand, the fully developed flow oscillation induces the oscillation of the effective temperature difference between the melt/solid interfaces (see Fig.9). When $\Delta\mathrm{T}$ is further increased, during the time period ($t = 2100 \sim 2156$ s), a new oscillation of $2T$ mode [30] appears, which produces the torsional oscillation (twisting) in the core of the flow. As shown in Fig.10, the $2T$ mode oscillation of low frequency ($f_l = 0.039$ Hz) enhances the oscillation amplitude of the indicator velocity, and modulates the 2+1 mode oscillation of relatively high frequency ($f_h = 0.72$ Hz). When the coexistence of two oscillation modes reaches the fully developed stage, the oscillation amplitude grows slowly, and the frequencies of the two oscillation modes gradually increase to $f_l = 0.05$ Hz and $f_h = 0.75$ Hz respectively (see Fig.11). Fig.3 also shows the evolution of indicator velocity against $\Delta\mathrm{T}$ for case-2. The behavior of the two-step Marangoni flow transitions is similar to the case-1. The first and second bifurcation points are $\Delta\mathrm{T} = 10.61$ K ($t = 68$ s) and $\Delta\mathrm{T} = 44.7$ K ($t = 286.9$ s) respectively, and the occurrences of the bifurcations are delayed. It may results from the time lag between the imposed temperature difference and the developments of the temperature and flow fields under the relatively fast heating velocity.

Fig.12 shows the evolutions of the azimuthal velocities at the monitor point against the effective temperature difference (ΔT_e). For case-1, when the effective temperature difference (ΔT_e) is 1.14 K, the local azimuthal velocity starts growth, and the first critical Marangoni number is estimated as Ma_{c1} = 15.68. For case-2, the first critical Marangoni number is estimated as Ma_{c1} = 20.19 (ΔT_e = 1.47 K). The second critical Marangoni number is determined through the indicator velocity. As shown in Fig.13, when ΔT_e is 5.95 K, the indicator velocity of case-1 starts oscillation with a frequency of f = 0.54 Hz by FFT analysis. The corresponding second critical Marangoni number is Ma_{c2} = 81.7. For case-2, the second critical Marangoni number is Ma_{c2} = 84.4 (ΔT_e = 6.15 K), and the corresponding oscillation frequency is f = 0.565 Hz. Fig.12 also indicates that the definition of the incipience of the oscillation is always accompanied with some uncertainty due to the transient imposed temperature difference. Fig.14 summaries the critical Marangoni numbers of the liquid bridges of low Pr number fluids as the function of aspect ratio [27-30,32]. The results are given by the current realistic model and by the simple model corresponding to the marginal stability limits. It can be seen that small heating velocity is beneficial to the accurate prediction of the critical Marangoni numbers.

5. Discussions

It is worthy to be noted that in the JAXA's experiment [31], the melt free surface temperatures is measured by three radiation thermometers, and four thermocouples were inserted in the cold disk to reveal the details of the oscillatory flow transition. On the other hand, to evaluate the possibility of using the same thermocouple arrangement to detect the first flow transition, Fig.15 shows the temperatures at four monitor points located at the melt/solid interface periphery (r = R) of the cold end. It can be seen that the first transition point predicted through the free surface temperature bifurcations is identical to that of the local azimuthal velocity (t = 303.5 s, see Fig.4). Fig.15 also shows the relative deviations of the temperatures at the four monitor points from the expected linear temperature decrease for the axisymmetric flow respectively. Fig. 15 indicates that the asymmetric temperature field grows rapidly during the time period of t = 303.5 ~ 340 s. At t = 340 s, the maximum temperature difference becomes about 0.01 K, which may possibly be detected through thermocouples of high sensitivity.

In the previous section, the second critical Marangoni number (t = 1655.2 s, Ma_{c2} = 81.7, f = 0.54 Hz) is predicted through the indicator velocity, which is sensitive to the occurrence of the oscillation of 2+1 mode. Fig.16 shows that the local free surface temperature starts oscillations at t = 1850 s (Ma = 90.6, f = 0.565 Hz) suggesting there is a large time lag from the incipience of the indicator velocity oscillation. However, in the JAXA's experiment, the onset of oscillatory Marangoni flow was detected through measuring melt free surface temperatures. Due to the limited sensitivity (0.1 K) of the measuring instruments, only the free surface temperature oscillations with low frequency and large amplitudes can be detected experimentally. Fig.17 shows the time evolution of the local free surface temperature. It can be seen that the amplitude of the free surface temperature oscillations corresponding to the 2+1 type mode predicted numerically is much smaller than the sensitivity of JAXA's measuring instruments. Judged from Fig.17, the experimentally detected free surface temperature oscillation (Ma_{c2} = 113, f = 0.02 Hz) may correspond to the incipience of the coexistence of 2+1 and 2T oscillation modes (t = 2120 s, Ma = 102.7, f = 0.039 Hz), and the corresponding low oscillation frequency of the free surface temperature may correspond to frequency of the 2T oscillation. Thus the JAXA's experiment may not have detected the exact critical condition, and very sensitive detecting system must be developed to determine the critical Marangoni numbers.

6. Conclusion

In the present study, a long-run numerical simulation was conducted on a realistic model of half-zone liquid bridge of molten tin, which is identical to the JAXA's experimental apparatus, and the critical Marangoni numbers are predicted. However, the definition of the incipience of the three-dimensional disturbance is always accompanied with some uncertainties due to the transient imposed temperature difference. Small heating velocity is beneficial to the accurate prediction of the critical Marangoni numbers. Moreover, the second critical Marangoni number predicted through free surface temperature oscillation is much larger than the one through the indicator velocity oscillation. The experimentally predicted second critical Marangoni number and critical frequency through free surface temperature may be much different from those numerically predicted due to the sensitivity of the experimental detection technique. The exact incipience of the oscillatory Marangoni flow is not easy to be observed through the free surface temperature unless a very sensitive temperature measurement system can be developed.

References

[1] D. Schwabe, in: H.C. Freyhardt (ED.), Crystals, Vol. 11, Springer, Berlin, 1988, 75.

[2] J. H Han, Z. W. Sun, L. R. Dai, J. C. Xie, W. R. Hu, J. Cryst. Growth, 169, 129-135 (1996)

[3] M. Levenstam, G. Amberg, T. Carlberg, M. Andersson, J. Cryst. Growth, 158(3), 24-30 (1996)

[4] S. Nakamura, T. Hibiya, K. Kakimoto, N. Imaishi, S. Nishizawa, A. Hirata, K. Mukai, S. Yoda, T. S. Morita, J. Crystal Growth, 186, 85-94 (1998)

[5] T. Hibiya, S. Nakamura, K. Mukai, Z.G. Niu, N. Imaishi, S. Nishizawa, S. Yoda, M. Koyama, Philos. Trans. Roy. Soc. London, Ser. A 356 (1739), 899-909 (1998)

[6] T. Hibiya, S. Nakamura, Advances in Space Research, 24, 1225-1230 (1999)

[7] M. Cheng, S. Kou, J. Crystal Growth, 218, 132-135 (2000)

[8] M. Sumiji, S. Nakamura, K. Onuma, T. Hibiya, Jpn. J. Applied Physics, Part 1, 39, 3688-3693 (2000)

[9] T. Azami, S. Nakamura, T. Hibiya, S. Nakamura, J. Crystal Growth, 223, 116-124 (2001)

[10] M. Sumiji, S. Nakamura, T. Azami, T. Hibiya, J. Crystal Growth, 223, 503-511 (2001)

[11] T. Azami, S. Nakamura, T. Hibiya, J. Crystal Growth, 231, 82-88 (2001)

[12] M. Sumiji, S. Nakamura, T. Hibiya, J. Crystal Growth, 235, 55-59 (2002)

[13] T. Azami, S. Nakamura, T. Hibiya, J. Jpn. Soc. Microgravity Appl. (in Japanese), 18, 16-25 (2001)

[14] T. Hibiya, S. Nakamura, T. Azami, M. Sumiji, N. Imaishi, K. Mukai, K. Onuma, S. Yoda, Acta Astronautica, 48, 71-78 (2001)

[15] Y. K. Yang, S. Kou, J. Crystal Growth, 222, 135-143 (2001)

[16] G.P. Neitzel, K.T. Chang, D.F. Jancowski, H.D. Mittelmann, Physics of Fluids, A5, 108-114 (1992)

[17] H.C. Kuhlmann, H.J. Rath, J. Fluid Mech., 247, 247-274 (1993)

[18] M. Wanschura, V. Shevtsova, H.C. Kuhlmann, H.J. Rath, Physics of Fluids, 5, 912-925 (1995)

[19] G. Chen, A. Lizee, B. Roux, J. Crystal Growth, 180, 238-647 (1998)

[20] Q.S. Chen, W.R. Hu, Int. J. Heat Mass Transfer, 41, 825-837 (1998)

[21] Q.S. Chen, W.R. Hu, V. Prasad, J. Crystal Growth, 203, 261-268 (1999)

[22] M. Levenstam, G. Amberg, W. Christian, Physics of Fluids, 13(4), 807-816 (2001)

[23] R. Rupp, G. Mueller, G. Neumann, J. Crystal Growth, 97, 34-41 (1989)

[24] M. Levenstam, G. Amberg, J. Fluid Mechanics, 297, 357–372 (1995)

[25] J. Leypoldt, H.C. Kuhlmann, H.J. Rath, J. Fluid Mech, 414, 285-314 (2000)

[26] M. Lappa, R. Savino, R. Monti, Int. J. Heat Mass Transfer, 44, 1983-2003 (2001)

[27] N. Imaishi, S. Yasushiro, T. Sato, S. Yoda, SPIE Proc. Vol. 3792 (Material Research in low gravity II), 344-352 (1999)

[28] N. Imaishi, S. Yasushiro, T. Sato, S. Yoda, Proc. of the 4th JSME-KSME Thermal Engineering Conference (Kobe), vol.3, 277-282 (2000)

[29] S. Yasushiro, T. Sato, N. Imaishi, S. Yoda, Space Forum, 6, 39-47 (2000)

[30] N. Imaishi, S. Yasuhiro, Y. Akiyama, S. Yoda, J. Crystal Growth, 230, 164-171 (2001)

[31] K. Takagi, M. Ohtaka, H. Natsui, T. Arai, S. Yoda, Z. Yuan, K. Mukai, S. Yasuhiro, N. Imaishi, J. Crystal Growth, 233, 399-407 (2001)

[32] S. Yasuhiro, K. Li, N. Imaishi Y. Akiyama, H. Natsui, S. Matsumoto, S. Yoda, J. Crystal Growth, 266, 152-159 (2004)

[33] S. Yasushiro, N. Imaishi, Y. Akiyama, S. Fujino, S. Yoda, J. Crystal Growth, 262, 631-644 (2004)

[34] T. Suzuki, H. Kawamura, J. Mech. Eng. Japan (in Japanese), 60-578(B), 58 (1994)

[35] H. Ozoe, K. Toh, J. Crystal Growth, 130, 645-656 (1993).

[36] S. Fujino, K. Miura, Kokyuroku of Research Institute of Mathematical Sciences (Kyoto University) (in Japanese), No.1265, 162-172 (2002)

Table 1　Thermophysical properties and geometric parameters.

		Molten Tin	Iron
Pr		0.009	-
Density	ρ [kg/m^3]	6793	7700
Thermal conductivity	k [W/mK]	35.44	20.0
Specific heat	C_p [J/kgK]	242	460
Viscosity	μ [kg/ms]	1.318×10^{-3}	-
Temperature gradient of surface tension	σ_T [N/mK]	-1.3×10^{-4}	-
Gravitational acceleration	g_0 [N/m]	9.8	-
Volumetric expansion coefficient	β [l/K]	1.3×10^{-4}.	-
Radius	R [m]	3.0×10^{-3}
Length of the liquid bridge	L [m]	3.66×10^{-3}
Length of rods	L$_r$ [m]	6.0×10^{-3}
Offset of the thermocouple junction from melt/rod interface d [m]		0.5×10^{-3}
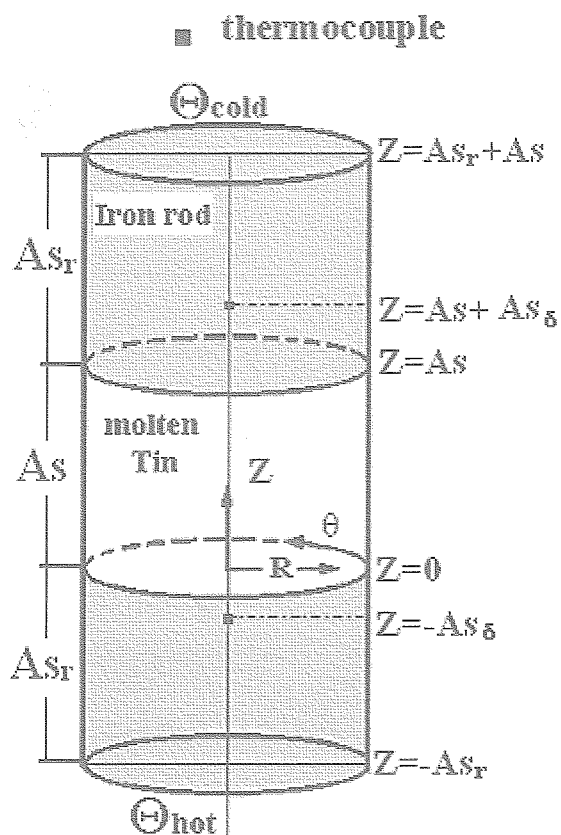
Fig.1.　Schematics of the realistic liquid bridge model including the supporting iron rods.
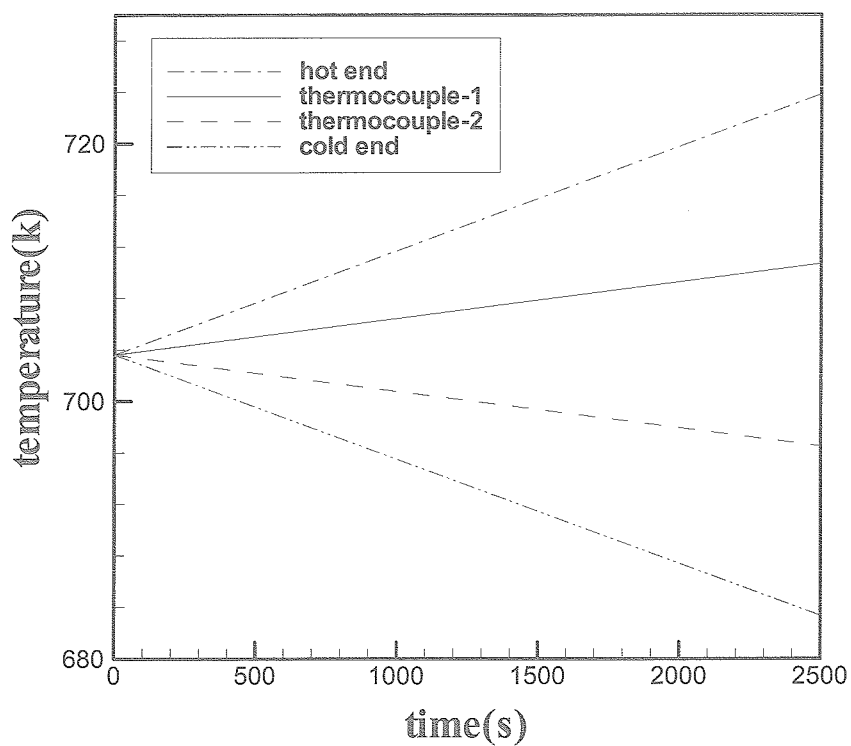
Fig.2.　Time evolutions of the simplified linear thermocouple temperatures and the converted imposed temperatures at the hot and cold end.
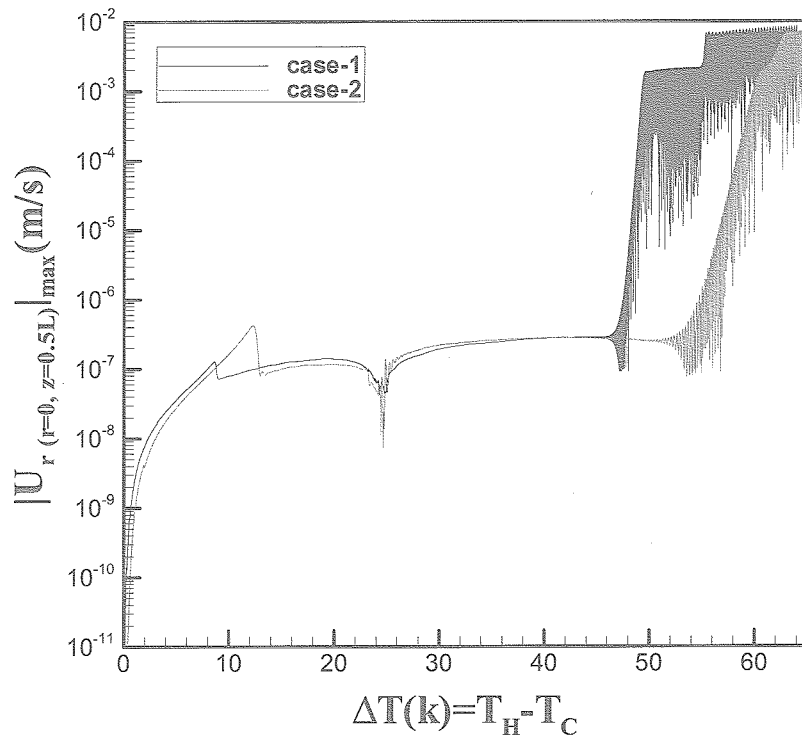
Fig.3 Evolution of the maximum absolute values of the radial velocity at the axis ($\left|U_{r(r=0,=0.5L)}\right|_{max}$) against the temperature difference between the hot and cold ends ($\Delta T = T_H - T_C$).
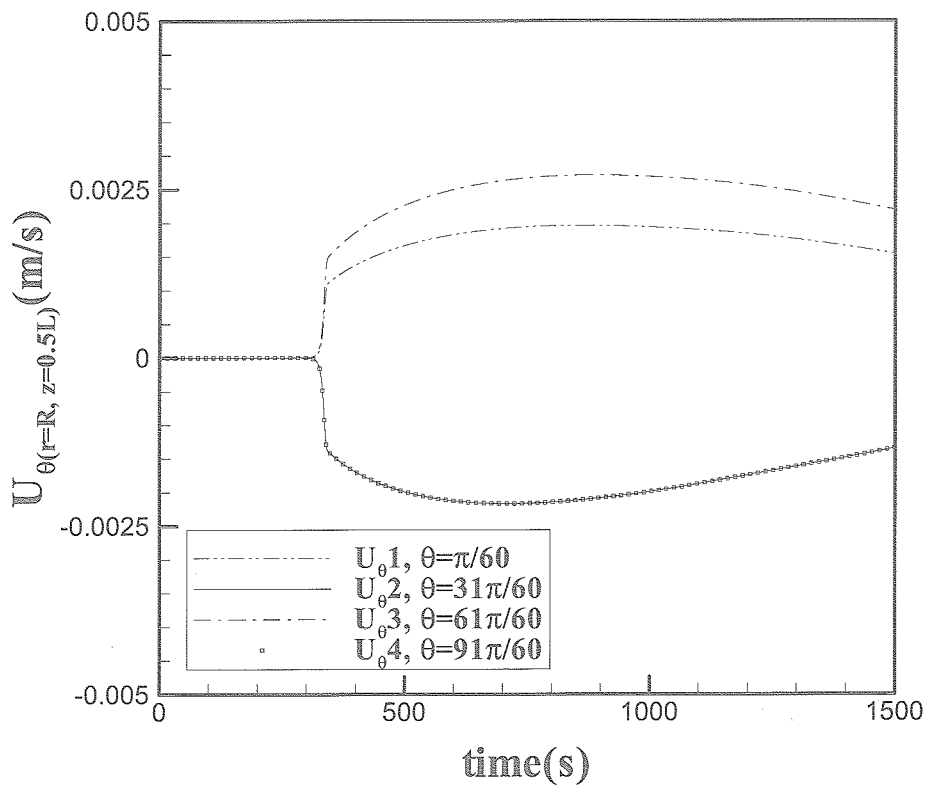
Fig.4. Time evolutions of the azimuthal velocity of the four monitor points at the melt free surface around the first critical point.
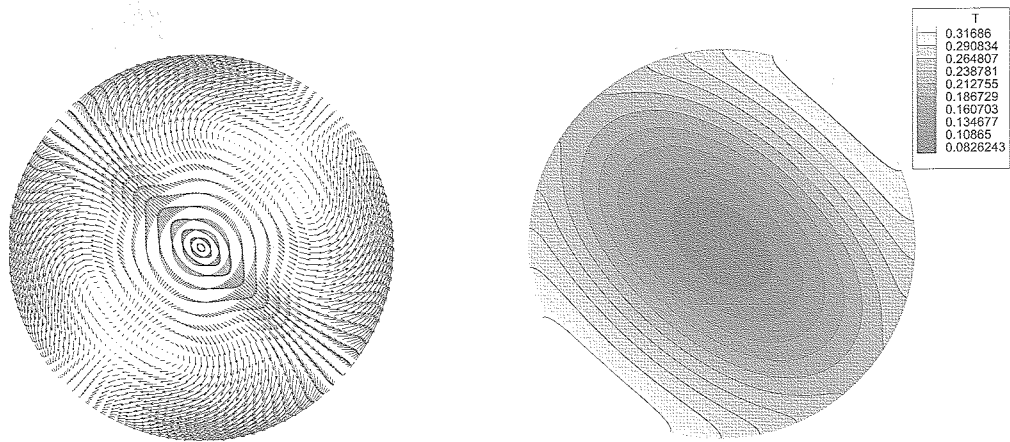
Fig. 5 Temperature and flow field cross sections (z = 0.5L) of the three-dimensional steady Marangoni flow of $m = 2$.
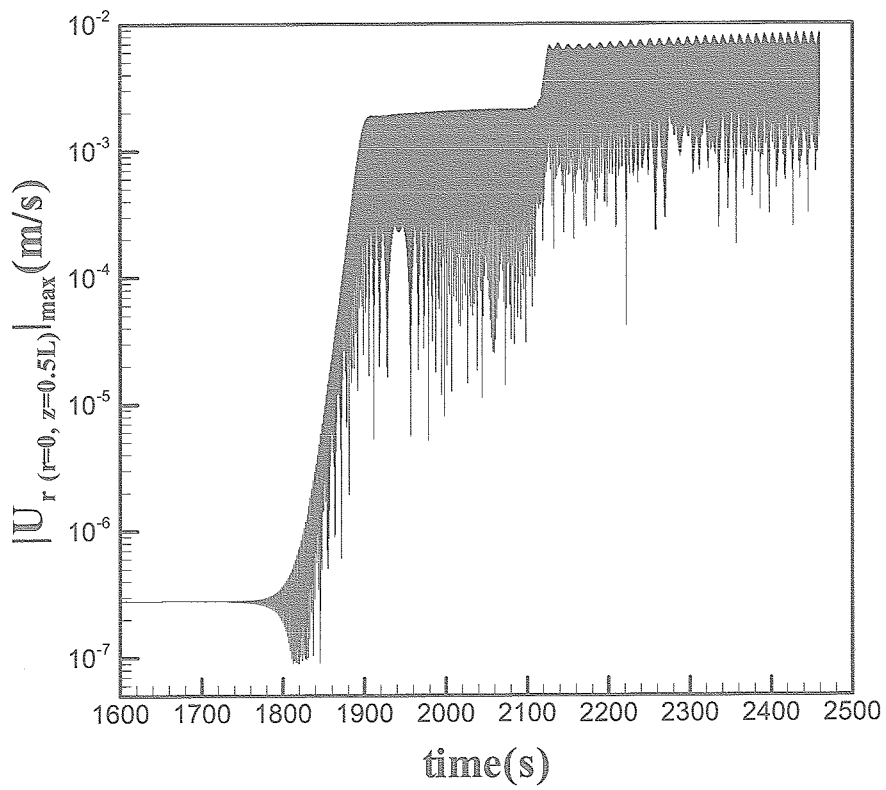
Fig.6. Time evolution of the maximum absolute value of the radial velocity at the axis ($\left| U_{r(r=0,=0.5L)} \right|_{max}$).

106
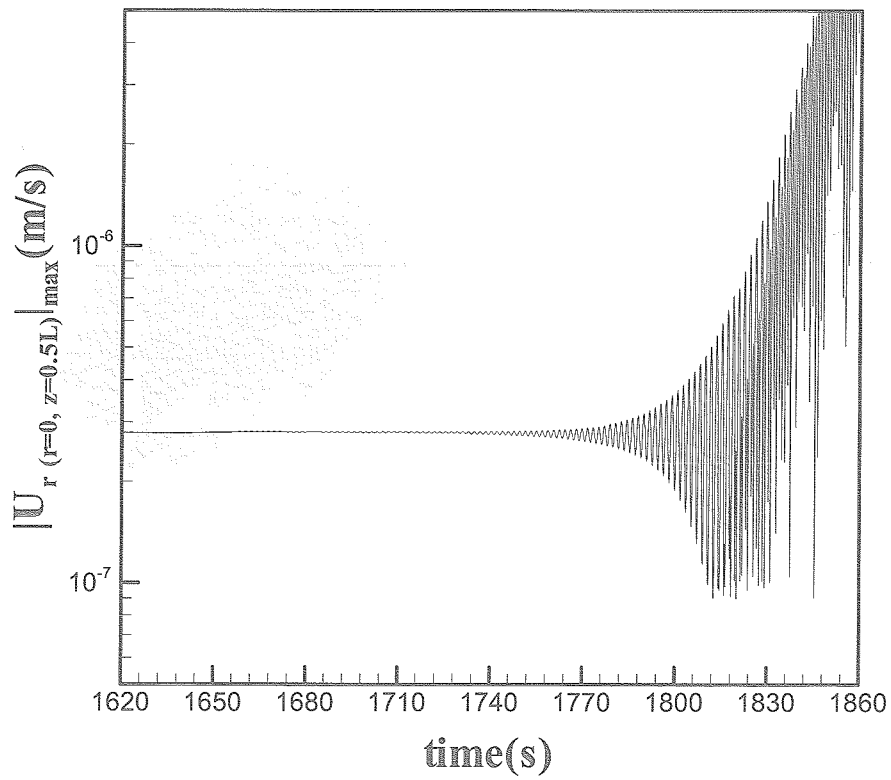
Fig.7. Time evolution of the maximum absolute value of the radial velocity at the axis ($\left| U_{r(r=0,=0.5L)} \right|_{max}$) around the second critical point.
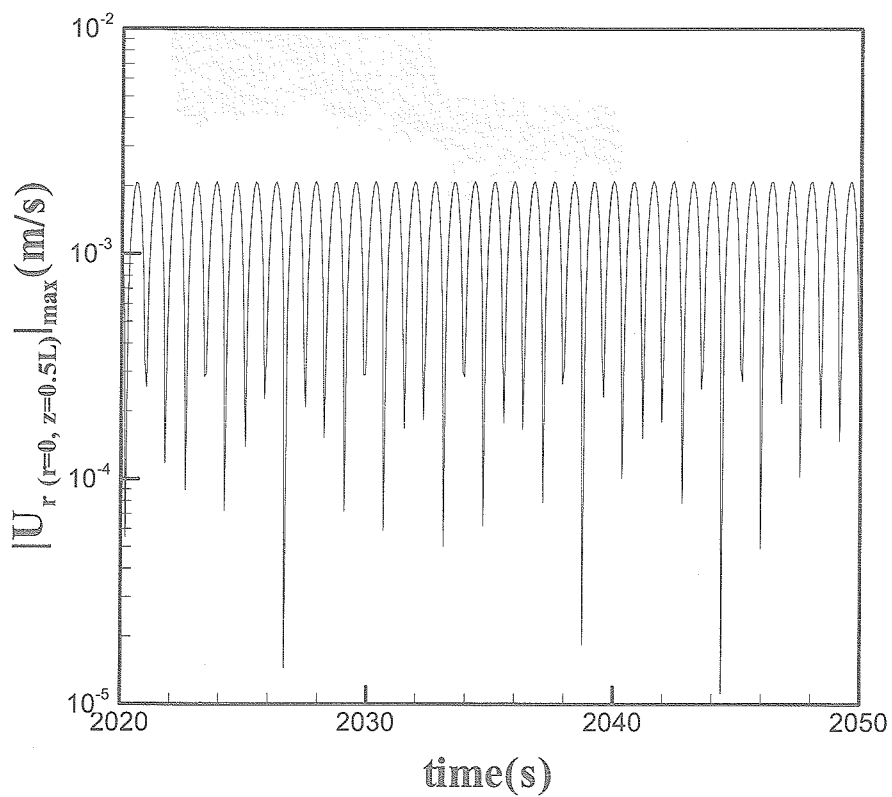
Fig.8. Time evolution of the maximum absolute value of the radial velocity at the axis ($\left| U_{r(r=0,=0.5L)} \right|_{max}$) for 2+1 oscillation.
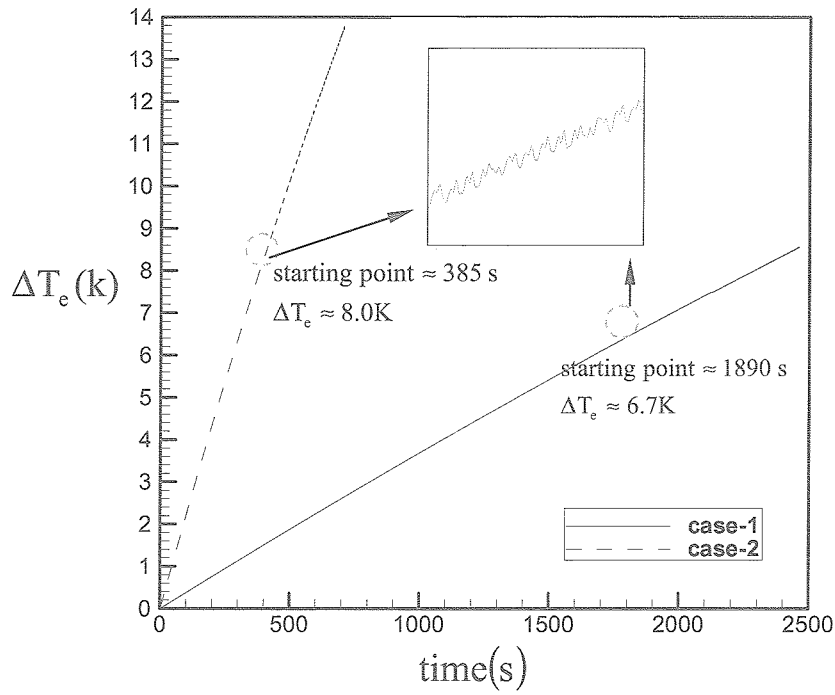
Fig.9. Time evolution of the effective temperature difference.
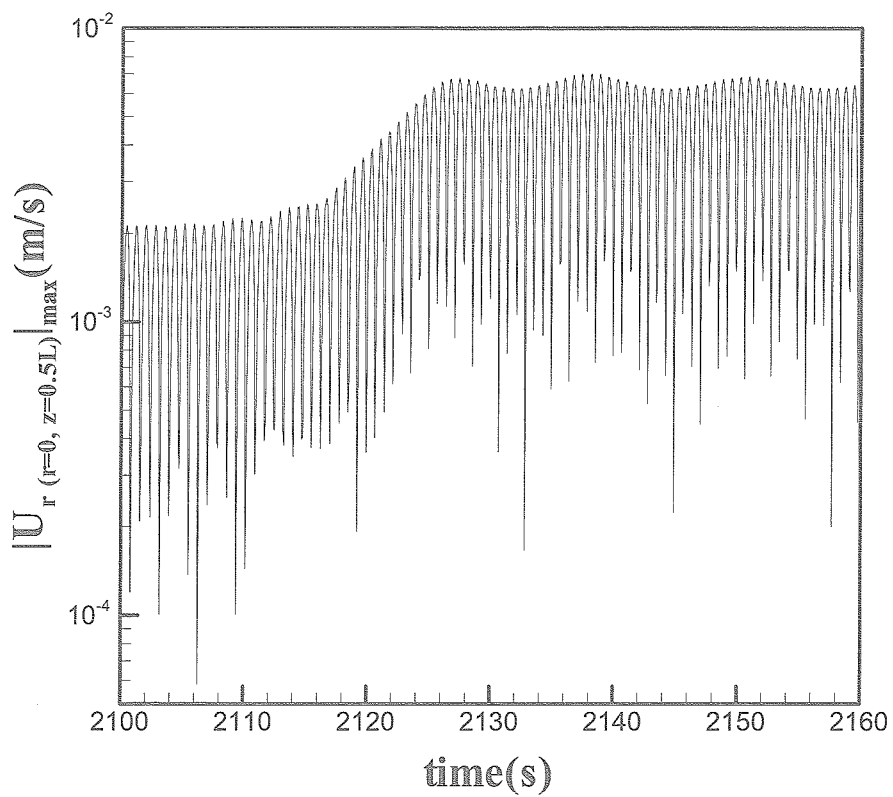
Fig.10. Time evolution of the maximum absolute value of the radial velocity at the axis ($\left| U_{r(r=0,=0.5L)} \right|_{max}$) for the transition from 2+1 oscillation to the coexistence of 2+1 and 2T oscillation.
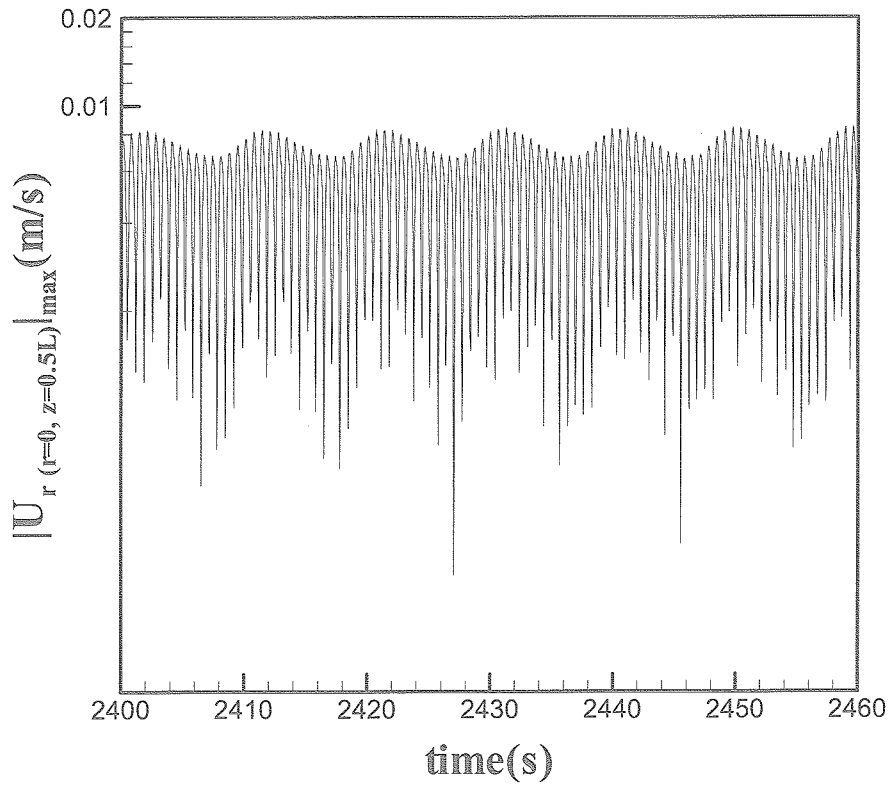
Fig.11. Time evolution of the maximum absolute value of the radial velocity at the axis ($\left|U_{r(r=0,=0.5L)}\right|_{max}$) for the coexistence of 2+1 and 2T oscillation.
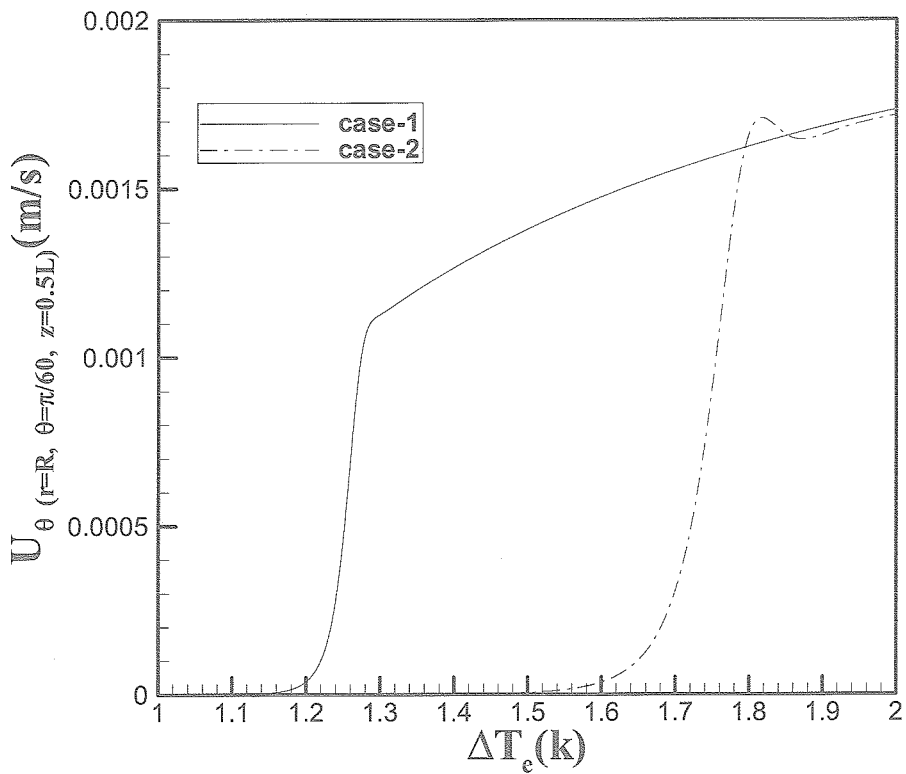

Fig.12. Evolutions of the azimuthal velocity of the monitor point at the melt free surface against the effective temperature difference around the first critical point.
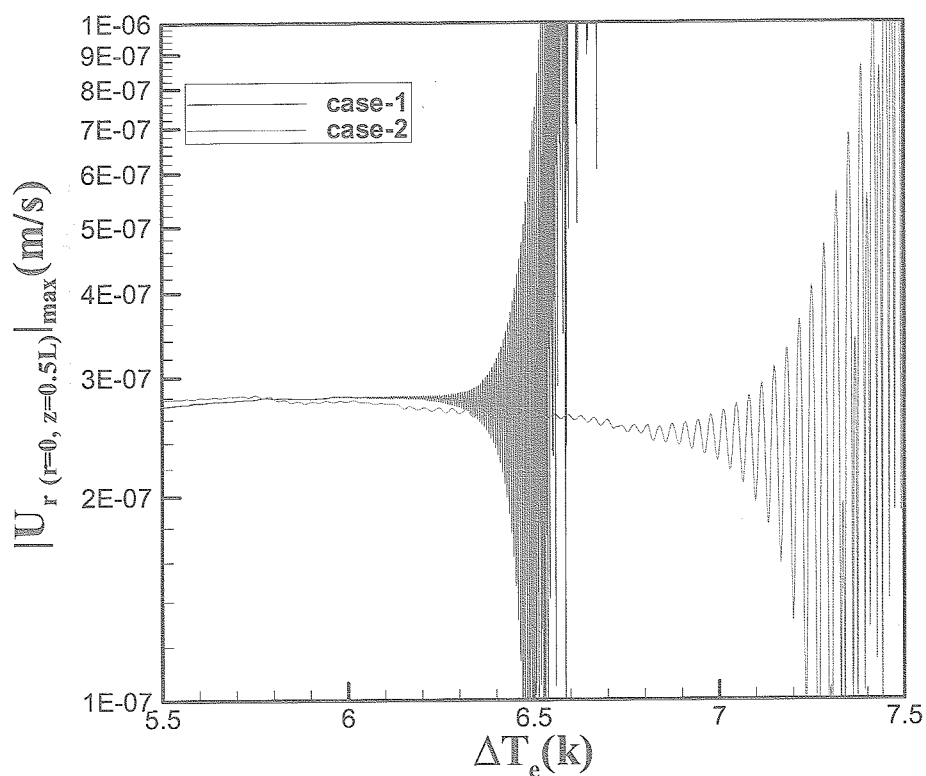
Fig.13. Evolutions of the maximum absolute value of the radial velocity at the axis ($\left|U_{r(r=0,=0.5L)}\right|_{max}$) against the effective temperature difference around the second critical point.
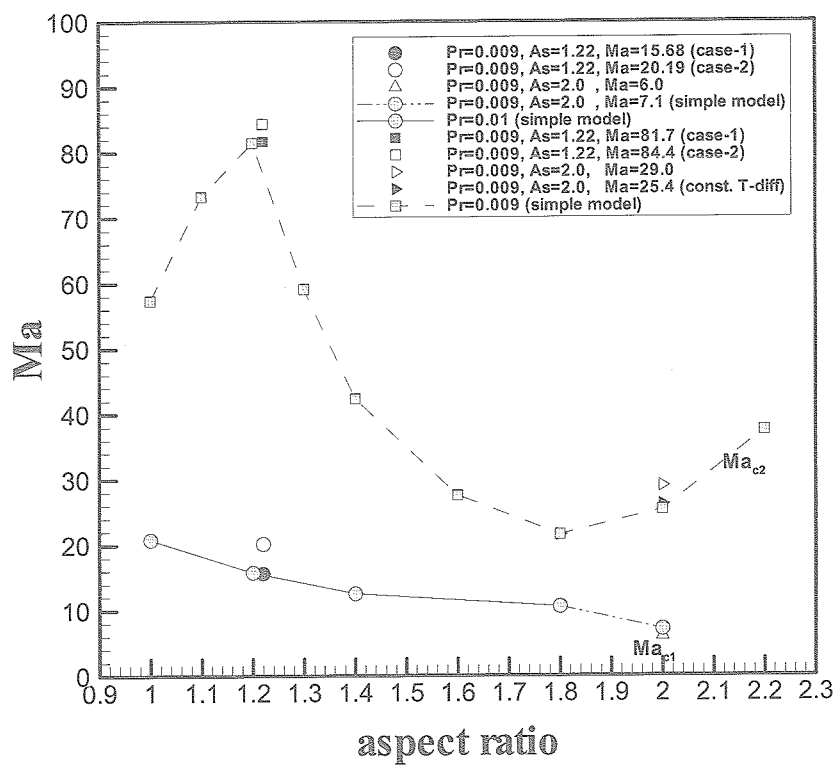

Fig.14. The critical Marangoni numbers of the liquid bridges of low Pr number fluids as the function of aspect ratio.

110
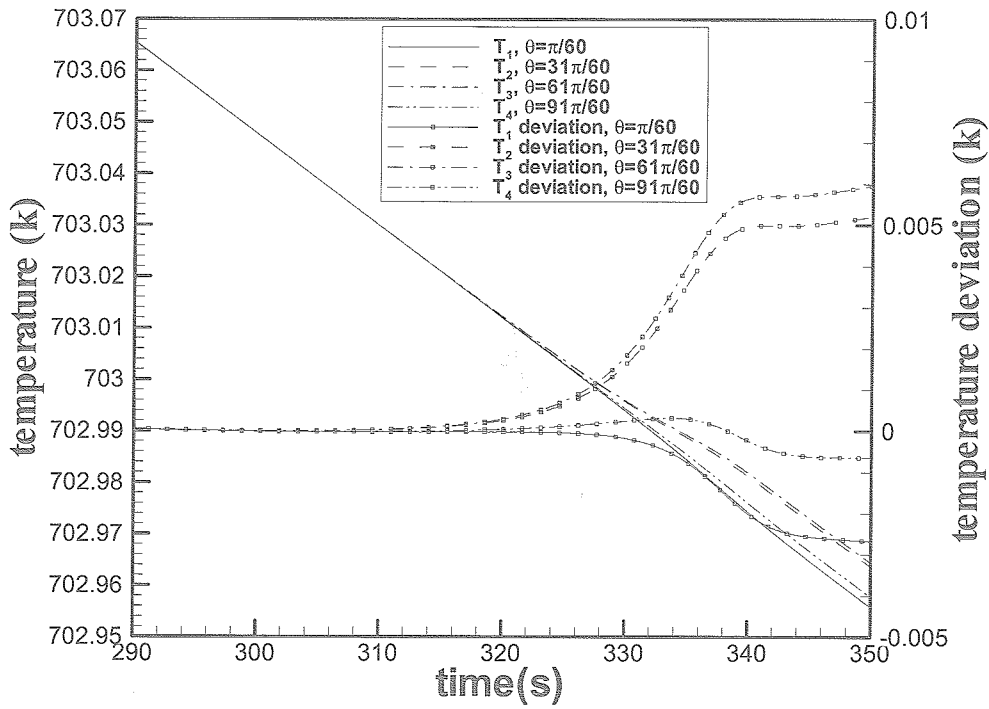
Fig.15. Time evolution of four monitor point temperature at the periphery of the melt/rod interface periphery on the cold side accompanied by the first flow transition.and their temperature deviations from the predicted temperature change for the axisymmetric flow system.
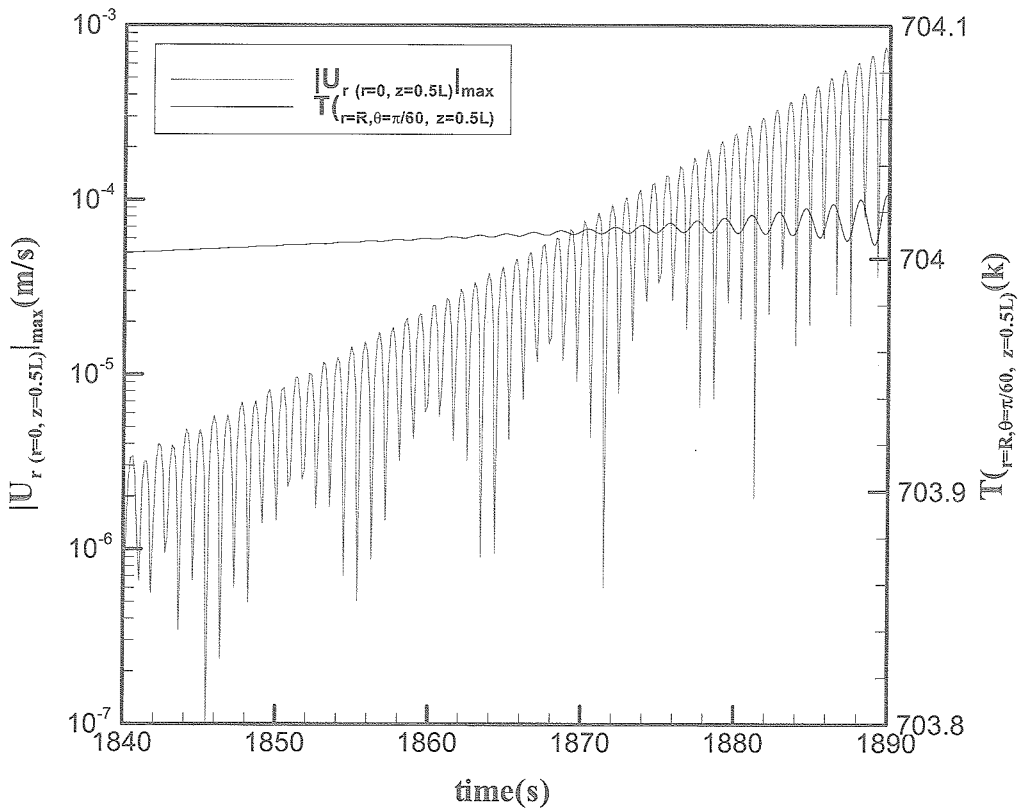

Fig.16. Time evolution of the free surface temperature of the monitor point at the melt free surface and the corresponding maximum absolute value of the radial velocity at the axis ($\left|U_{r(r=0,=0.5L)}\right|_{max}$) around incipience of free surface temperature oscillation.

Fig.17.   Time evolution of the free surface temperature of the monitor point at the melt free surface.